
Article:
Laird, Alison Monica orcid.org/0000-0003-0423-363X, Akers, Charles, Riley, Joscelin et al. (2 more authors) (2020) First measurement in the Gamow window of a reaction for the γ-process in inverse kinematics: 76Se(α, γ)80Kr. Physics Letters B. 135575. ISSN: 0370-2693

https://doi.org/10.1016/j.physletb.2020.135575

First measurement in the Gamow window of a reaction for the γ-process in inverse kinematics: ^{76}Se$(\alpha,\gamma)^{80}$Kr

J. Fallis[a], C. Akers[b,a,1,*], A. M. Laird[b], A. Simon[c], A. Spyrou[e,f,g], G. Christian[a,2], D. Connolly[d,3], U. Hager[d,4], D. A. Hutcheon[a], A. Lennarz[a], P. O'Malley[d,5], S. J. Quinn[e,f,g], J. Riley[b], A. Rojas[a], C. Ruiz[a], M. Williams[b,a]

[a] *TRIUMF, Vancouver, British Columbia V6T 2A3, Canada*
[b] *Department of Physics, University of York, York, YO10 5DD, UK*
[c] *Department of Physics, University of Notre Dame, Notre Dame, IN 46556, USA*
[d] *Department of Physics, Colorado School of Mines, Golden, CO 80401, USA*
[e] *National Superconducting Cyclotron Laboratory, Michigan State University, East Lansing, Michigan 48824, USA*
[f] *Department of Physics & Astronomy, Michigan State University, East Lansing, Michigan 48824, USA*
[g] *Joint Institute of Nuclear Astrophysics, Michigan State University, East Lansing, Michigan 48824, USA*

Abstract

The p-nuclei are the few stable nuclei heavier than iron on the neutron-deficient side of the valley of stability that cannot be produced through astrophysical neutron-capture reactions. The limited experimental data on reactions through which the p-nuclei might be produced leaves the origin of their production largely unknown. This work presents the first cross section measurements of the ^{76}Se$(\alpha,\gamma)^{80}$Kr reaction. The rate of the time reversed reaction, ^{80}Kr$(\gamma,\alpha)^{76}$Se, is one of the most uncertain of possible reactions which can occur at the ^{80}Kr branching point on the γ-process photo-disintegration pathway. The reaction flow through ^{80}Kr will directly affect the final abundance of the p nuclide ^{78}Kr. Experimental cross sections at two astrophysically relevant energies are reported and compared to cross sections calculated using Hauser-Feshbach codes TALYS, NON-SMOKER, and SMARAGD. The success of these first (α,γ) cross section measurements performed in inverse kinematics in the energy region of the γ-process opens the door for future studies of reactions on radioactive γ-process nuclides.

1. Introduction

Of the elements heavier than iron, some of the most interesting isotopes also happen to be among the least abundant. The *p-nuclei* are a collection of stable isotopes heavier than iron, which sit along the neutron, n, deficient side of the valley of stability, and which cannot be produced by the known n-capture processes (the r-, and s-processes). The production of these p-nuclei requires a separate astrophysical process which is commonly called the p-process [1, 2]. While several astrophysical sites and nucleosynthesis pathways have been proposed, it is not yet clear which (or which combination) is responsible for their production. Recent work of Travaglio et al. [3] for the first time employed Galactic Chemical Evolution models with metallicity-dependent core collapse supernovae yields to investigate the contributions of those various sites to the solar abundances of the p-nuclei.

Previously, one of the favoured scenarios for p-nuclei production was a supernova shock-front passing through the O-Ne layer of a massive star undergoing core-collapse [4, 5, 6, 7]. The p-nuclei

*Corresponding author
Email address: cakers@ibs.re.kr (C. Akers)
[1]Present address: Rare Isotope Science Project, Institute for Basic Science, Daejeon 34000, Republic of Korea
[2]Present address: Department of Astronomy and Physics, St. Mary's University, Halifax, Nova Scotia B3H 3C3, Canada
[3]Present address: Los Alamos National Laboratory, Los Alamos, NM 87545, USA
[4]Present address: Department of Physics & Astronomy, Michigan State University, East Lansing, Michigan 48824, USA
[5]Present address: Department of Physics, University of Notre Dame, Notre Dame, IN 46556, USA

may be produced when pre-existing heavy seed-nuclei undergo photo-disintegration reactions due to the high temperatures in this environment (1.7 to 3.3 GK [7]). To distinguish this process from the other p-process candidates, this mechanism is referred to as the γ-process. However, the exact production site, or sites, remain uncertain, with Type 1A supernovae also currently favoured.

At the start of the γ-process, (γ, n) reactions dominate, driving the reaction flow to n-deficient isotopes of the same element. However, at some point the rate of the (γ, p) and/or the (γ, α) reactions exceed the rate of the (γ, n) reactions and the reaction flow is deflected to the isotopic chain of a lighter element [1, 4, 7, 8]. These *branching points* and the relative rates of all their associated reactions are critical nuclear inputs when studying any scenario and its resulting isotopic abundances. Currently very few of the reactions relevant to the γ-process have been studied experimentally and, among these, there are no data for radiative capture reactions on radioactive nuclei. While predictions from Hauser-Feshbach (HF) model codes can provide some guidance where experimental reaction data are lacking, there are often large uncertainties associated as the predicted values vary significantly based on the choice of model inputs. For (γ, α) reactions, the variation in the α optical model potentials (αOMP) is particularly significant (see Fig. 2 and Ref. [9, 10]). With scarce α-capture data at energies relevant for the γ-process being available to-date, continuous experimental efforts in the mass and energy range of the γ-process are needed to better constrain the theory.

One γ-process branching point occurs at ^{80}Kr and the resulting reaction flow will directly affect the abundance of the p-nuclide ^{78}Kr [6]. Of the three possible photo-disintegration reactions which can occur, $^{80}\mathrm{Kr}(\gamma, \alpha)^{76}\mathrm{Se}$ is currently the most uncertain. Therefore, the time reversed reaction, $^{76}\mathrm{Se}(\alpha, \gamma)^{80}\mathrm{Kr}$, was identified as a priority measurement for γ-process studies [6].

This letter presents the first cross section measurements of $^{76}\mathrm{Se}(\alpha, \gamma)^{80}\mathrm{Kr}$. These measurements were performed at energies below the (p,n) channel threshold, where the sensitivity to the level density and the γ-ray strength function is less prominent, allowing for constraint of the α optical potential model directly at energies relevant to the γ-process. Moreover, these are the first measurements of a γ-process reaction performed in inverse kinematics in the Gamow window. Previous work, including Glorius et al. [11] who recently reported on the measurement of $^{124}\mathrm{Xe}(p,\gamma)^{125}\mathrm{Cs}$, have been conducted at energies just above the Gamow window. Given that much of the γ-process reaction flow involves unstable nuclei, inverse kinematic techniques will be critical for future γ-process studies (see Ref. [12] for current status of γ-process (p, γ) measurements in inverse kinematics).

2. Experimental details

The DRAGON [13, 14, 15] recoil separator used in this work is located in the ISAC facility [16] at TRIUMF. DRAGON is designed to study radiative proton and α capture reactions at sub-Coulomb barrier energies in inverse kinematics. It is comprised of three main sections: (i) a windowless differentially pumped gas target; (ii) a high-supression two-stage separator; and (iii) a recoil detector system. The separator consists primarily of two sets of magnetic and electric dipoles. The recoil detector system, located downstream of the final focus of the separator, is comprised of two microchannel plate detectors (MCPs), used for measuring local and separator time of flight (TOF), and a segmented anode ionization chamber (IC), used for measuring recoil energy loss.

DRAGON's windowless gas target was filled with helium gas at a pressure between $10.6 - 11.1$ mbar throughout the experiment. The target's effective length has previously been measured to be 12.3(5) cm [17]. Two silicon detectors were located inside of the target chamber to monitor the α particles elastically scattered by the incoming beam for the purposes of beam normalization. There was also an array of 30 high-efficiency Bismuth Germanate (BGO) detectors surrounding the chamber which were used for detecting γ rays coincident with recoil events. The beam current was monitored with absolute Faraday cup (FC) readings up and downstream of the target, which were taken every hour at the start and end of every run.

Downstream of the separator, two MCPs measured the secondary electron emission from ions traversing the diamond-like carbon foils placed in the beamline. The foils were sufficiently thin ($20\ \mu\mathrm{g/cm}^2$) so that the MCPs could be used in tandem with the IC located immediately downstream of them. The time difference between the prompt-γ detection from the BGO array and the recoil MCP detection allowed for the separator TOF to be cal-

culated. See Refs. [18, 19] for more details on this detection system.

A beam of $^{76}Se^{12+}$, produced from a 74% enriched ^{76}Se sample placed in the ISAC Off-line Ion Source [20], was impinged on the windowless gas target with an average intensity of 2×10^{10} s^{-1}. The beam was accelerated to energies of $E_{\rm beam} = 1.513(3)$A MeV ($E_{\rm c.m.} = 5.749(12)$ MeV) and 1.434(3)A MeV (5.449(12) MeV). These energies were chosen as they are within the Gamow energy window ($E_{\rm c.m.} = 3.6 - 8.7$ MeV) of the γ-process. Downstream of the target, before the separator's optical elements, a 350 nm aluminum stripper foil was used to increase the average charge state of the beam and recoils [15]. The ^{80}Kr recoils were then separated from the unreacted beam using DRAGON's separator [13, 14, 21].

Given that DRAGON was specifically designed to study explosive nucleosynthesis with beams of mass A $\leq$ 30, this measurement of ^{76}Se$(\alpha,\gamma)^{80}$Kr represents a significant departure in beam and recoil masses. The commissioning work to establish the feasibility of the new techniques employed here was reported in Ref. [22].

3. Analysis

To determine the experimental recoil yield per incident ion (Y) at each energy, the total number of recoil events ($N_{\rm r}^{\rm tot}$) was divided by the total number of incident beam particles ($N_{\rm b}$). In order to calculate $N_{\rm r}^{\rm tot}$ the number of detected recoil events $N_{\rm r}^{\rm det}$ was divided by all of the separator and detector efficiencies. The yield is then as follows:

$$Y = \frac{N_{\rm r}^{\rm det}}{N_{\rm b}\,\eta_{\rm BGO}\,\eta_{\rm CSF}\,\eta_{\rm t}\,\eta_{\rm MCP}\,\eta_{\rm det}\,\eta_{\rm live}}, \qquad (1)$$

where $\eta_{\rm BGO}$ is the the BGO γ detection efficiency, $\eta_{\rm CSF}$ is the charge state fraction for the selected recoil charge state, $\eta_{\rm t}$ is the separator transmission, $\eta_{\rm MCP}$ is the MCP TOF detection efficiency, $\eta_{\rm det}$ is the combined MCP foil transmission and IC detection efficiency, and $\eta_{\rm live}$ is the live-time of the data acquisition system. The experimental yield was then used to determine the experimental cross section (σ). As the level density at the measured energies was expected to be high, multiple resonances were expected to be present in the target region and thus the cross section was calculated as an effective cross section, integrated across the energy range of the target:

$$\sigma = Y \left(\frac{N_{\rm t}}{A}\right)^{-1}, \qquad (2)$$

where $N_{\rm t}/A$ is the target density per unit area.

All $N_{\rm r}^{\rm det}$, $N_{\rm b}$ and efficiency values are given in table 1.

3.1. Beam normalization and energy

To determine $N_{\rm b}$, beam normalization was performed using the procedure laid out in Ref. [23]. This involved calculating a normalization value that related the number of elastic scattering events detected in the silicon detectors to the number of incident beam ions, using Faraday cups located up and downstream of the target. The number of events detected in the silicon detectors could then subsequently be used to calculate the number of incident beam ions for any given run.

Due to the low charge state of the incoming beam and the limited electric rigidity of DRAGON's electric dipoles, the beam energy could not be measured directly as is typically done [14]. Instead, the beam energy was measured after passing through the target and stripper foil. The initial beam energy was then calculated based on energy loss data from SRIM [24]. This resulted in an uncertainty in $E_{\rm c.m.}$ of 12 keV due to uncertainty in the SRIM data and target thickness.

3.2. Recoil charge state distribution and transmission

The recoils transmitted to the end detector were all in the 25+ charge state which was the most abundantly populated charge state that could be transmitted through the separator[6]. The charge state fractions (CSF) were measured experimentally using beams of $^{84}Kr^{14+}$. As these charge state measurements also needed to encompass future ^{76}Se$(\alpha,\gamma)^{80}$Kr measurements, CSF were measured at five beam energies from 1.12 to 1.53 MeV/nucleon. The CSF presented in Table 1 ($\eta_{\rm CSF}$) were interpolated from a second order polynomial fit to these data. The uncertainties are taken from the weighted average of the difference between the fit and the measurements.

[6]The 25+ charge state was not expected to be the most abundantly populated however, but lower, more intense charge states could not be transmitted through the electric dipoles due to their limited electric rigidity

Table 1: The number of recoil events detected ($N_{\rm r}^{\rm det}$), integrated beam on target ($N_{\rm b}$), center of mass energy ($E_{\rm c.m.}$), energy spread across the target ($\Delta E_{\rm c.m.}$), and system efficiencies calculated for each data group. Note that the high energy data is separated into two groups as the separator tune was changed during the run to help reduce the rate of beam events at the end detectors.

(MeV)				(%)					
$E_{\rm c.m.}$	$\Delta E_{\rm c.m.}$	$N_{\rm r}^{\rm det}$	$N_{\rm b}$ ($\times 10^{15}$)	$\eta_{\rm BGO}$	$\eta_{\rm CSF}$	$\eta_{\rm t}$	$\eta_{\rm MCP}$	$\eta_{\rm det}$	$\eta_{\rm live}$
5.713(12)	0.072(5)	46(7)	0.659(21)	80(11)	2.11(6)	98.8(14)	99.67(12)	58(4)	94.5(4)
5.713(12)	0.072(5)	201(16)	1.31(4)	80(11)	2.11(6)	98.8(14)	99.67(12)	58(4)	83.7(4)
5.415(12)	0.072(5)	86(19)	4.31(14)	80(11)	1.63(6)	98.8(14)	99.70(6)	59(4)	84.8(4)

The recoil cone angle was calculated to be <3 mrad, well within DRAGON's acceptance of <20 mrad [13]. The recoil separator transmission was hence very high, calculated as 98.75% for both beam energies using a GEANT 3 simulation.

3.3. Detector efficiencies and live time

The detection efficiency of the BGO array ($\eta_{\rm BGO}$) depended on the energy and multiplicity of the γ-rays produced during the reaction. As the actual γ cascades from the populated excited states in ^{80}Kr are not known, the maximum and minimum efficiencies were determined from GEANT4 simulations [25, 26]. The minimum efficiency (65%) occurs if the excited state emits a single γ-ray directly to the ground state. The maximum efficiency (95%) occurs if the cascade contains the largest possible number of γ-rays with energies above the detection threshold (1 MeV). These values were the same for both incident beam energies. The BGO array efficiency was then taken to be 80(11)%, where the uncertainty is a combination of 68% coverage of the efficiency range and the uncertainty inherent in the simulation [26, 27].

The detection efficiency of the MCP TOF system ($\eta_{\rm MCP}$) and of the IC ($\eta_{\rm det}$) was determined using attenuated beam data, as described in Ref. [28].

The system live time ($\eta_{\rm live}$) was determined using the procedure described in Ref. [29]. Table 1 contains the complete tabulated set of efficiency values.

3.4. Particle identification

With a standard tune, the unsuppressed beam rate was high enough to overwhelm the IC. Reducing the voltage of the second electrostatic dipole by a small amount ($\leq 1.4\%$) significantly reduced the rate of beam events at the end detectors. GEANT3 simulations [13] for these deliberate mistunes indicate no reduction in separator transmission, $\eta_{\rm t}$.

Identification of ^{80}Kr recoils from the unsuppressed beam events was performed by applying

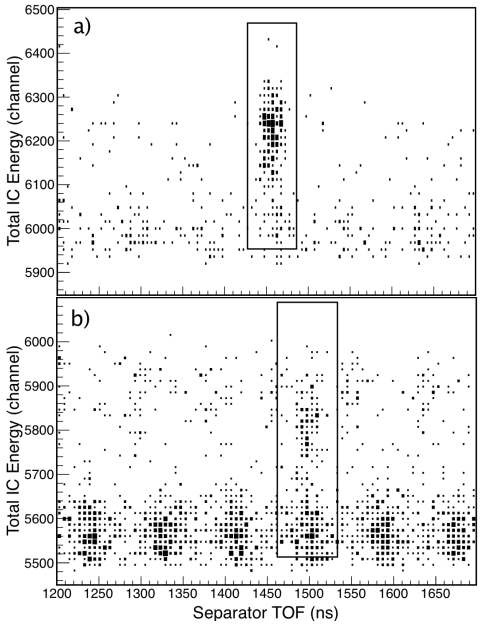

Figure 1: Plot of total IC energy vs. separator TOF for data passing additional software cuts (see text) for a) E_{cm}=5.713 MeV and b) E_{cm}=5.415 MeV data. The IC energy and separator TOF cuts showing the regions of interest are also indicated.

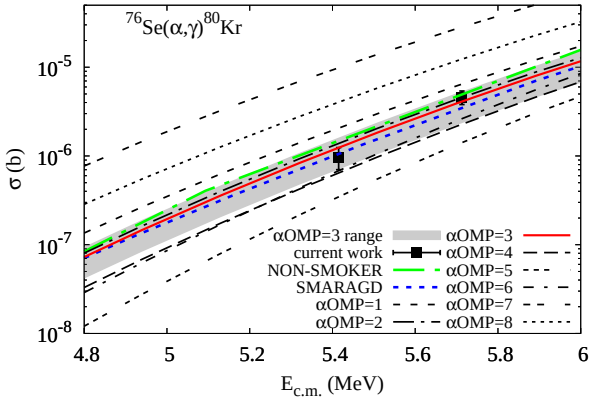

Figure 2: Cross section data obtain in this work compared with those calculated with TALYS, SMARAGD, and NON-SMOKER. The gray-shaded area denotes range of uncertainty in the cross section from αOMP=3 obtained by scaling up and down the red curve to overlap with the 68% confidence level of the experimental data.

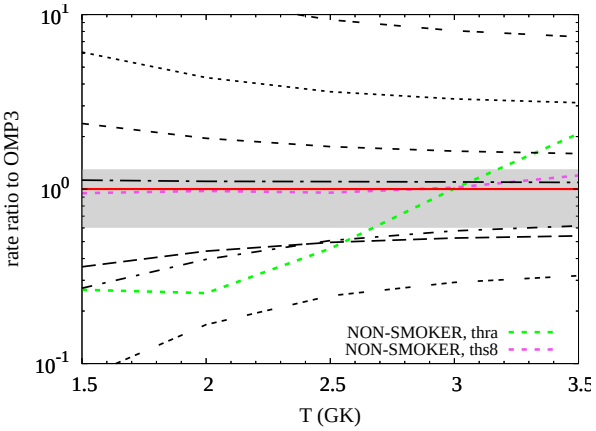

Figure 3: Ratio of reaction rates from Talys to that obtained with αOMP=3. Line styles and colors correspond to those used in Fig. 2. The green and magenta dashed lines indicate rates from REACLIB database that correspond to two different parametrizations of the NON-SMOKER results. See text for details. The gray shaded area correspond to the uncertainty in the αOMP=3 cross section. SMARAGD reaction rate data was not avaliable.

cuts on the total IC energy, the energy loss in each of the four IC anodes, local TOF using the MCP, and the TOF through the separator (time between coincident γ-ray and MCP events). The clearest particle identification was then seen in a plot of the total IC energy vs. the separator TOF (Fig. 1). The regions of interest (ROIs) indicated in Fig. 1 represent the IC energy and separator TOF cuts. For each energy N_r^{det} is the number of events in the cut, minus the calculated background (Table 1). Due to the time structure of the bunched beam, background events did not have a completely random separator TOF (as seen in Fig. 1b); they appeared in packets separated by 84.8 ns. To properly determine this background, the recoil cut was displaced along the separator TOF axis in periods of this magnitude, multiple times. The number of background events within these cuts was then averaged to give the expected number of background events inside the ROIs.

4. Results and discussion

The beam intensities, recoil counts, and efficiencies presented in Table 1 resulted in cross sections of 4.6(8) μbarn and 0.97(27) μbarn at $E_{c.m.}$ = 5.713(12) MeV and 5.415(12) MeV centre-of-target energies, respectively. A direct comparison of the experimental cross sections with a number of Hauser-Feshbach (HF) cross sections, σ_{HF}, calculated using NON-SMOKER, SMARAGD [30] and TALYS is presented in Fig. 2.

The calculated σ_{HF} depend on both the code used and choice of input parameters. Eight sets of σ_{HF} are calculated using the TALYS code version 1.9 [31] (TL) for each available α-optical potential model αOMP: 1) Koning-Delaroche [32], 2) McFadden-Satchler [33], 3) Table 1 in Demetriou et al. [34], 4) Table 2 in Ref. [34], 5) a dispersive model in Ref. [34], 6) Avrigeanu [35], 7) Nolte [36], and 8) Avrigeanu [37]. Within the energy range covered by this work, the α-capture cross section models do not show strong dependence on the level density and the γ-ray strength functions (γSF) implemented in the calculations. At most the resulting cross sections changed by 23%, thus these parameters were kept constant through the calculations and were set to the constant temperature matched to the Fermi gas model [38] for the level density and the Kopecky-Uhl generalized Lorentzian [39] for the γSF to match those of the NON-SMOKER code for better comparison.

It can be seen in Figure 2 that the results of NON-SMOKER are in a good agreement with the higher-energy data point while overestimating the lower-energy point. Cross sections obtained from a new version of the NON-SMOKER code, SMARAGD, tend to underestimate the higher-energy point, while they overlap with the lower-energy data. The results of TALYS calculations, span nearly two orders

of magnitude for various models of the αOMP available through the code. The results obtained with αOMP=2 , i.e. the McFadden-Satchler potential, which is used in the NON-SMOKER code, are similar to those of NON-SMOKER. Only the results for αOMP=3, i.e., that of Demetriou et al. [34] show an agreement with both experimental data points simultaneously to within their 68% confidence level. The gray-shaded area in Figure 2 indicates the uncertainty range of the HF cross section obtained by scaling the cross section for αOMP=3 up and down to match the experimental uncertainties. The scaling factors were 1.3 and 1.7 for the upper and lower limits, respectively. That substantially reduced the uncertainty in the cross section predictions from the HF calculations, which is typically quoted to be a factor of 10 for the α-capture reactions. The results for αOMP=2 and both NON-SMOKER and SMARAGD fall within that uncertainty range as well.

From the HF input parameters used for the cross sections, the reaction rates for the ^{76}Se(α,γ)^{80}Kr were derived. The recommended rate was calculated using the αOMP=3 model. Figure 3 shows ratios of the rates calculated with TALYS relative to the recommended one. The shaded area corresponds to the range of uncertainty in the recommended rate that stems from the uncertainty in the calculated cross section. The color and style of the lines corresponds to that of Figure 2. Additionally, two evaluations of the reaction rate from NON-SMOKER taken from the REACLIB database are shown in Figure 3: the recommended rate "th8" [40] and the rate from the parameterized fit to NON-SMOKER calculations "thra" [41]. It should be noted, that as expected the results for αOPM=2 and the recommended REACLIB rate fall within the uncertainty range. The parametrized fit to the NON-SMOKER data significantly deviates from the recommended rate, however, it is unclear from [41] whether the discrepancy is due to the fit precision or due to changes in the rate calculations between references [40] and [41]. The values of the recommended rate for the ^{76}Se(α,γ)^{80}Kr reaction within the γ-process Gamow window are listed in Table 2 together with the lower and upper limits.

The rates of the forward reactions can be used to calculate the reverse, photodisintegration rates in order to determine at what temperatures the ^{80}Kr(γ,α)^{76}Se rate will dominate over the ^{80}Kr(γ,n)^{79}Kr, allowing for direct feeding of the p-nucleus ^{76}Se and bypassing ^{78}Kr. For that purpose, for the same input parameters used for the direct rates in TALYS the reverse ones were calculated for the (γ,α), (γ,n) and (γ,p) channels. Since the level densities and γ-ray strengths were not varied, the uncertainties for the neutron and proton emission rates (which do not depend on the αOMP model) were assumed to have the same uncertainty as the calculated α-capture cross section of this work. The results are indicated by the dashed bands in Figure 4. If all the αOMP models were taken into account, the range of predicted rates corresponds to the gray-shaded area. The red band represents the uncertainty in the rate that originates from the uncertainty in our α-capture cross section data. The rates are plotted as ratios to the (γ,n) rate. From the ratio, the temperature at which the α emission becomes dominant can be estimated. If the total uncertainty of the TALYS rates is used, the uncertainty in the temperature spans 1.6-2.6 GK. With the reduced uncertainty of this work, that range is 1.9-2.2 GK.

Table 2: Reaction rates for the ^{76}Se(α,γ)^{80}Kr reaction obtained from the TALYS using the αOMP=3 potential. The upper and lower limits correspond to the uncertainty in the HF cross section indicated in Figure 2.

T	$N_A<\sigma\nu>$ (cm^3 s^{-1} mol^{-1})		
	recommended	lower limit	upper limit
1.5	1.46×10^{-12}	8.79×10^{-13}	1.90×10^{-12}
2	3.71×10^{-9}	2.22×10^{-9}	4.82×10^{-9}
2.5	7.88×10^{-7}	4.73×10^{-7}	1.02×10^{-6}
3	3.50×10^{-5}	2.10×10^{-5}	4.56×10^{-5}
3.5	5.51×10^{-4}	3.31×10^{-4}	7.16×10^{-4}

5. Conclusions

In conclusion, the first measurement of cross sections for ^{76}Se(α,γ)^{80}Kr at γ-process energies have been obtained in inverse kinematics using a recoil separator. There is just a hand-full of available (α,γ) data in the $75 \leq A < 90$ mass region, thus this measurement provides an important insight to the α-capture cross sections in the region of the lightest p-nuclei. The measured cross sections were best matched by TALYS predictions using the αOMP3 from Table 1 in Demetriou et al. [34] with an uncertainty band of about 30%. The σ_{HF} obtained with the potential of McFadden and Satchler [33] with both SMARAGD and TALYS codes fell within that uncertainty range. This is

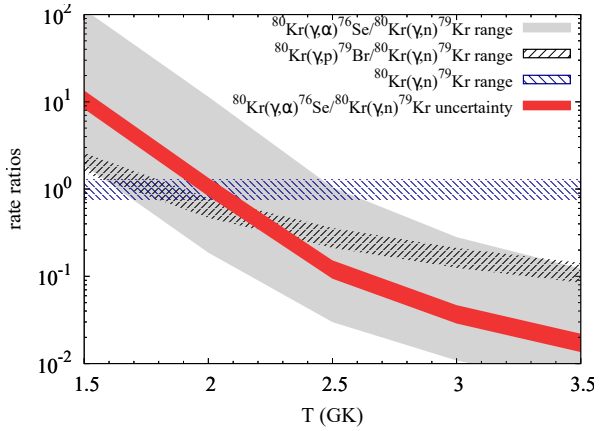

Figure 4: Ratios of (γ,α) and (γ,p) rates to (γ,n) rates obtained with Talys. Gray shaded band is the uncertainty in the $(\gamma,\alpha)/(\gamma,n)$ ratio obtained from Talys. The red band corresponds to the $(\gamma,\alpha)/(\gamma,n)$ ratio resulting from this work. The dashed regions indicate the $(\gamma,p)/(\gamma,n)$ ratio (black) and the uncertainty in the (γ,n) rate (blue).

consistent with the results of Ref. [9] which found that $\sigma_{\rm HF}$ from the TALYS code using the αOMP from Table 1 in Demetriou et al. [34] (αOMP3) resulted in the smallest average discrepancy from the data across all the stable Ni isotopes and consistently reproduces the α-capture cross sections across the γ-process nuclei [10]. Reaction rates from models with $\sigma_{\rm HF}$ consistent with this work all differed by less than a factor of 1.3 for temperatures from $1-3.5$ GK, a significant reduction from the most commonly presumed factor of 10 for (α,γ) reactions in the p-process mass region. Additionally, this work reduces by a factor of at least 3 the uncertainty in the temperature at which the ^{80}Kr$(\gamma,\alpha)^{76}$Se reaction becomes the dominant photo-disintegration pathway from ^{80}Kr in the γ-process. With the updated rates, the γ-process scenario will feed the production of ^{76}Se only at the temperatures below 1.9-2.2 GK, at higher temperature the $(\gamma$,n) channel will feed the production of ^{78}Kr.

The success of this measurement is due to the unique combination of the low beam energies available from the ISAC facility, the windowless gas target technology developed for DRAGON, and the beam suppression achieved using the DRAGON separator. This method may then provide an increased sensitivity to cross section measurements at lower energies compared to in-beam and activation measurements performed in regular kinematics. This is particularly applicable when, as in the present case, the isotope of interest results in chemically unstable targets. Also, due to the short half-lives involved, any future studies of reactions on radioactive isotopes will need to be performed in inverse kinematics. The demonstration of this technique at γ-process masses and energies opens the door for measurements using radioactive beams and will allow future studies of $(\alpha,\ \gamma)$ reactions on the unstable isotopes in the γ-process.

6. Acknowledgments

The authors thank the ISAC operations and technical staff at TRIUMF. TRIUMF's core operations are supported via a contribution from the federal government through the National Research Council Canada, and the Government of British Columbia provides building capital funds. DRAGON is supported by funds from the National Sciences and Engineering Research Council of Canada. CA, AML, and JR acknowledge the support of the UK Science and Technology Facilities Council (STFC). This work was supported in part by the National Science Foundation under Grant numbers PHY-1614442 and PHY-1430152 (JINA-CEE). The author would like to thank T. Rauscher for providing the cross section calculations from the SMARAGD code, and P. Mohr for useful discussions.

References

[1] M. Arnould, S. Goriely, Phys. Rep. 384 (2003) 1.
[2] T. Rauscher, N. Dauphas, I. Dillmann, C. Fröhlich, Z. Fülöp, G. Gyürky, Reports on Progress in Physics 76 (6) (2013) 066201.
[3] C. Travaglio, T. Rauscher, A. Heger, M. Pignatari, C. West, The Astrophysical Journal 854 (1) (2018) 18.
[4] M. Rayet, M. Arnould, N. Prantzos, Astro. Astrophys. 227 (1990) 271–281.
[5] M. Rayet, M. Arnould, M. Hashimoto, N. Prantzos, K. Nomoto, Astro. Astrophys. 298 (1995) 517.
[6] T. Rauscher, Phys. Rev. C 73 (1) (2006) 015804.
[7] W. Rapp, J. Görres, M. Wiescher, H. Schatz, F. Käppeler, Astrophys. J. 653 (2006) 474–489.
[8] T. Rauscher, A. Heger, R. D. Hoffman, S. E. Woosley, Astrophys. J. 576 (2002) 323–348.
[9] A. Simon, M. Beard, A. Spyrou, S. J. Quinn, B. Bucher, M. Couder, P. A. DeYoung, A. C. Dombos, J. Görres, A. Kontos, A. Long, M. T. Moran, N. Paul, J. Pereira, D. Robertson, K. Smith, E. Stech, R. Talwar, W. P. Tan, M. Wiescher, Phys. Rev. C 92 (2) (2015) 025806.
[10] A. Simon, M. Beard, B. S. Meyer, B. Roach, Journal of Physics G: Nuclear and Particle Physics 44 (6) (2017) 064006.

[11] J. Glorius, C. Langer, Z. Slavkovská, L. Bott, C. Brandau, B. Brückner, K. Blaum, X. Chen, S. Dababneh, T. Davinson, P. Erbacher, S. Fiebiger, T. Gaßner, K. Göbel, M. Groothuis, A. Gumberidze, G. Gyürky, M. Heil, R. Hess, R. Hensch, P. Hillmann, P.-M. Hillenbrand, O. Hinrichs, B. Jurado, T. Kausch, A. Khodaparast, T. Kisselbach, N. Klapper, C. Kozhuharov, D. Kurtulgil, G. Lane, C. Lederer-Woods, M. Lestinsky, S. Litvinov, Y. A. Litvinov, B. Löher, F. Nolden, N. Petridis, U. Popp, T. Rauscher, M. Reed, R. Reifarth, M. S. Sanjari, D. Savran, H. Simon, U. Spillmann, M. Steck, T. Stöhlker, J. Stumm, A. Surzhykov, T. Szücs, T. T. Nguyen, A. Taremi Zadeh, B. Thomas, S. Y. Torilov, H. Törnqvist, M. Träger, C. Trageser, S. Trotsenko, L. Varga, M. Volknandt, H. Weick, M. Weigand, C. Wolf, P. J. Woods, Y. M. Xing, Phys. Rev. Lett. 122 (2019) 092701.

[12] B. Mei *et al.*, Phys. Rev. C 92 (3) (2015) 035803.

[13] D. A. Hutcheon, S. Bishop, L. Buchmann, M. L. Chatterjee, A. A. Chen, J. M. D'Auria, S. Engel, D. Gigliotti, U. Greife, D. Hunter, A. Hussein, C. C. Jewett, N. Khan, M. Lamey, A. M. Laird, W. Liu, A. Olin, D. Ottewell, J. G. Rogers, G. Roy, H. Sprenger, C. Wrede, Nucl. Instrum. and Methods in Phys. Res. A 498 (2003) 190–210.

[14] S. Engel, D. Hutcheon, S. Bishop, L. Buchmann, J. Caggiano, M. L. Chatterjee, A. A. Chen, J. D'Auria, D. Gigliotti, U. Greife, D. Hunter, A. Hussein, C. C. Jewett, A. M. Laird, M. Lamey, W. Liu, A. Olin, D. Ottewell, J. Pearson, C. Ruiz, G. Ruprecht, M. Trinczek, C. Vockenhuber, C. Wrede, Nucl. Instrum. and Methods in Phys. Res. A 553 (2005) 491–500.

[15] C. Vockenhuber, C. O. Ouellet, L. Buchmann, J. Caggiano, A. A. Chen, J. M. D'Auria, D. Frekers, A. Hussein, D. A. Hutcheon, W. Kutschera, K. Jayamanna, D. Ottewell, M. Paul, J. Pearson, C. Ruiz, G. Ruprecht, M. Trinczek, A. Wallner, Nucl. Instrum. and Methods in Phys. Res. B 259 (2007) 688–693.

[16] J. Dilling, R. Krücken, L. Merminga (Eds.), ISAC and ARIEL: the TRIUMF Radioactive Beam Facilities and the Scientific Program, Springer, New York, 2014, previously published as *Hyperfine Interactions*, Volume 225, 2014.

[17] D. A. Hutcheon, C. Ruiz, J. Fallis, J. M. D'Auria, B. Davids, U. Hager, L. Martin, D. F. Ottewell, S. Reeve, A. Rojas, Nucl. Instrum. and Methods in Phys. Res. A 689 (2012) 70–74.

[18] C. Vockenhuber, L. Buchmann, J. Caggiano, A. A. Chen, J. M. D'Auria, C. A. Davis, U. Greife, A. Hussein, D. A. Hutcheon, D. Ottewell, C. O. Ouellet, A. Parikh, J. Pearson, C. Ruiz, G. Ruprecht, M. Trinczek, J. Zylberberg, Nucl. Instrum. and Methods in Phys. Res. B 266 (2008) 4167–4170.

[19] C. Vockenhuber, L. E. Erikson, L. Buchmann, U. Greife, U. Hager, D. A. Hutcheon, M. Lamey, P. Machule, D. Ottewell, C. Ruiz, G. Ruprecht, Nucl. Instrum. and Methods in Phys. Res. A 603 (2009) 372–378.

[20] K. Jayamanna, Hyperfine Interactions 225 (2014) 51–62.

[21] D. A. Hutcheon, L. Buchmann, A. A. Chen, J. M. D'Auria, C. A. Davis, U. Greife, A. Hussein, D. F. Ottewell, C. V. Ouellet, A. Parikh, P. Parker, J. Pearson, C. Ruiz, G. Ruprecht, M. Trinczek, C. Vockenhuber, Nucl. Instrum. and Methods in Phys. Res. B 266 (2008) 4171–4175.

[22] A. Simon, J. Fallis, A. Spyrou, A. M. Laird, C. Ruiz, L. Buchmann, B. R. Fulton, D. Hutcheon, L. Martin, D. Ottewell, A. Rojas, European Physical Journal A 49 (2013) 60.

[23] J. M. D'Auria, R. E. Azuma, S. Bishop, L. Buchmann, M. L. Chatterjee, A. A. Chen, S. Engel, D. Gigliotti, U. Greife, D. Hunter, A. Hussein, D. Hutcheon, C. C. Jewett, J. José, J. D. King, A. M. Laird, M. Lamey, R. Lewis, W. Liu, A. Olin, D. Ottewell, P. Parker, J. Rogers, C. Ruiz, M. Trinczek, C. Wrede, Phys. Rev. C 69 (6) (2004) 065803.

[24] J. F. Ziegler, M. Ziegler, J. Biersack, Nucl. Instrum. and Methods in Phys. Res. B 268 (11-12) (2010) 1818 – 1823.

[25] S. Agostinelli *et al.*, Nucl. Instrum. and Methods in Phys. Res. A 506 (3) (2003) 250 – 303.

[26] C. Akers, Ph.D. thesis, University of York, York, UK (2015).

[27] D. G. Gigliotti, Master's thesis, University of Northern British Columbia, BC, Canada (2004).

[28] C. Akers, A. M. Laird, B. R. Fulton, C. Ruiz, D. W. Bardayan, L. Buchmann, G. Christian, B. Davids, L. Erikson, J. Fallis, U. Hager, D. Hutcheon, L. Martin, A. S. J. Murphy, K. Nelson, D. Ottewell, A. Rojas, A. Spyrou, Phys. Rev. C 94 (2016) 065803.

[29] G. Christian, C. Akers, D. Connolly, J. Fallis, D. Hutcheon, K. Olchanski, C. Ruiz, European Physical Journal A 50 (2014) 75. arXiv:1403.3425.

[30] T. Rauscher, Int. J. Mod. Phys. E 20 (2011) 1071–1169.

[31] A. Koning, S. Hilaire, M. Duijvestijn, Talys-1.0, Proc. of the Int. Conf. Nucl. Data for Sci. Tech. - ND2007, May 22 - 27, 2007, Nice (2008) 211.

[32] A. Koning, J. Delaroche, Nucl. Phys. A 713 (2003) 231.

[33] L. McFadden, G. Satchler, Nucl. Phys. 84 (1966) 177.

[34] P. Demetriou, C. Grama, S. Goriely, Nucl. Phys. A 707 (2002) 253.

[35] V. Avrigeanu, M. Avrigeanu, C. Mănăilescu, Physical Review C 90 (4) (2014) 044612.

[36] M. Nolte, H. Machner, J. Bojowald, Physical Review C 36 (4) (1987) 1312–1316.

[37] V. Avrigeanu, P. E. Hodgson, M. Avrigeanu, Physical Review C 49 (4) (1994) 2136–2141.

[38] A. Gilbert, A. Cameron, Can. J. Phys. 43 (1965) 1446.

[39] J. Kopecky, M. Uhl, Phys. Rev. C 41 (1990) 1941.

[40] R. H. Cyburt, A. M. Amthor, R. Ferguson, Z. Meisel, K. Smith, S. Warren, A. Heger, R. D. Hoffman, T. Rauscher, A. Sakharuk, H. Schatz, F. K. Thielemann, M. Wiescher, Astrophys. J Suppl. S 189 (2010) 240–252.

[41] T. Rauscher, F.-K. Thielemann, Atomic Data and Nuclear Data Tables 75 (1) (2000) 1 – 351.